

Adaptive space-time finite element methods for non-autonomous parabolic problems with distributional sources

Ulrich Langer, Andreas Schafelner

March 23, 2020

Abstract

We consider locally stabilized, conforming finite element schemes on completely unstructured simplicial space-time meshes for the numerical solution of parabolic initial-boundary value problems with variable, possibly discontinuous in space and time, coefficients. Distributional sources are also admitted. Discontinuous coefficients, non-smooth boundaries, changing boundary conditions, non-smooth or incompatible initial conditions, and non-smooth right-hand sides can lead to non-smooth solutions. We present new a priori and a posteriori error estimates for low-regularity solutions. In order to avoid reduced convergence rates appearing in the case of uniform mesh refinement, we also consider adaptive refinement procedures based on residual a posteriori error indicators and functional a posteriori error estimators. The huge system of space-time finite element equations is then solved by means of GMRES preconditioned by space-time algebraic multigrid. In particular, in the 4d space-time case that is 3d in space, simultaneous space-time parallelization can considerably reduce the computational time. We present and discuss numerical results for several examples possessing different regularity features.

Keywords: Non-autonomous parabolic initial-boundary value problem, distributional sources, space-time finite element methods, unstructured meshes, adaptivity

1 Introduction

Time-parallel and space-time methods, in particular, space-time finite element methods have a long history. We refer the interested reader to the survey articles [14] and [36] for a comprehensive review of time-parallel and space-time methods, respectively. We here only mention the Streamline Upwind Petrov Galerkin (SUPG) finite element method (sometimes also called Streamline Diffusion (SD) method), that was originally proposed by Hughes and Brooks for solving stationary convection-dominated convection-diffusion problems [16], and

was later used by Johnson and Saranen [9] to construct stable finite element schemes for time-dependent convection-diffusion problems, discretizing space and time simultaneously in time-slices. Similarly, in [17], Hughes, Franca and Hulbert proposed and analyzed the more general Galerkin/Least-Squares Finite Element Method (FEM) for stationary and instationary problems including time-dependent convection-diffusion problems. Both techniques were then used in many publications to stabilize finite element schemes. The revival of space-time methods is certainly connected with the availability of massively parallel computers with thousands or even millions of cores, but also with the simultaneous adaptivity in space and time, the easy handling of moving spatial domains and interfaces that are fixed in the space-time domain Q , and the all-at-once treatment of first-order optimality conditions (KKT system) in optimal control problems with parabolic or hyperbolic PDE constraints. Recently, time-upwind stabilizations have been used to construct and analyze coercive space-time Isogeometric Analysis (IGA) schemes in [23], partial low-rank tensor IGA schemes [26], and space-time hp -finite element schemes combined with mesh-grading in time to treat singularities in time [11]. These papers rely on a tensor-product structure of space and time. Results related to methods that do not assume a tensor-product structure were presented, e.g., in [34], where the author proposes and analyzes a inf-sup-stable space-time FEM on completely unstructured decompositions of the space-time domain, and in [1], where an arbitrary dimension convection-diffusion scheme for space-time problems is proposed, with two different discretizations. Unstructured space-time finite element and IGA methods have also been used to solve involved engineering problems; see, e.g., [2, 18], and the references therein, where mostly unstructured meshes are used within time slabs into which the space-time cylinder Q is decomposed. Following our previous work [24], we will derive, analyze and test space-time finite element methods on completely unstructured simplicial space-time meshes for non-autonomous parabolic initial-boundary value problems with distributional right-hand sides of the form: find u such that

$$\partial_t u - \operatorname{div}_x(\nu \nabla_x u) = f - \operatorname{div}_x(\mathbf{f}) \quad \text{in } Q = \Omega \times (0, T), \quad (1)$$

$$u = u_D := 0 \quad \text{on } \Sigma = \partial\Omega \times (0, T), \quad (2)$$

$$u = u_0 \quad \text{on } \Sigma_0 = \Omega \times \{0\}, \quad (3)$$

where the spatial domain $\Omega \subset \mathbb{R}^d$, $d = 1, 2, 3$, is bounded and Lipschitz, $T > 0$ denotes the final time, $\nu \in L_\infty(Q)$ is a given uniformly bounded and positive coefficient that may discontinuously depend on the spatial variable $x = (x_1, \dots, x_d)$ and the time variable t , $f \in L_2(Q)$, and $\mathbf{f} \in [L_2(Q)]^d$. If $\mathbf{f} = \mathbf{0}$ and ν is of bounded variation in t for almost all x , then the weak solution u of (1)–(3) has maximal parabolic regularity, i.e., $\partial_t u \in L_2(Q)$ and $\mathcal{L}_x u := -\operatorname{div}_x(\nu \nabla_x u) \in L_2(Q)$, see [12]. Thus, in the maximal parabolic regularity setting, the PDE $\partial_t u - \operatorname{div}_x(\nu \nabla_x u) = f$ makes sense in $L_2(Q)$, and this setting was the starting point for deriving the consistent space-time finite element schemes in [24]. If $\mathbf{f} \neq \mathbf{0}$ and it is not smooth enough, i.e., \mathbf{f} creates a distribution that is not in $L_2(Q)$, then maximal parabolic regularity does not

hold. However, in many applications, the vector field \mathbf{f} has a special structure. For instance, in 2d eddy current problems, ν denotes the reluctivity, f is nothing but the impressed current in the coils, and \mathbf{f} represents the magnetization in the permanent magnets. In such a way, we can model a rotating electrical machine, see, e.g., [29]. Motivated by such applications, we can assume that there is a decomposition of the space-time cylinder $\overline{Q} = \bigcup_{i=1}^m \overline{Q}_i$ into m non-overlapping, sufficiently smooth subdomains Q_1, \dots, Q_m such that \mathbf{f} is sufficiently smooth in Q_i but may have jumps across the boundaries of these subdomains. These jumps create distributions located on the interfaces between the subdomains. In this paper, we consider exactly this case of such a special right-hand side with a piecewise smooth vector-field \mathbf{f} leading to a distribution that is located on the interfaces. We again derive a consistent space-time finite element scheme, for which we prove a best-approximation (Céa-like) estimate that immediately yields convergence rate estimates in terms of the mesh-size h under additional regularity assumptions. In the case of low-regularity solutions, say, $u \in H^{1+s}(Q)$ with some $s \in (0, 1]$, and uniform mesh refinement, we can only expect a convergence rate of $O(h^s)$ in the corresponding energy norm independent of the polynomial order p of the finite element shape functions used. To circumvent this loss in the convergence rate, we also consider full space-time adaptive finite element procedures based on residual indicators or functional error estimators. We compare the efficiency of these adaptive approaches in a series of numerical experiments.

The remainder of the paper is organized as follows. In Section 2, we recall the standard space-time variational formulation and solvability results including maximal parabolic regularity and other regularity results. Section 3 is devoted to the derivation of consistent space-time finite element schemes. New a priori error estimates are presented in Section 4. Section 5 deals with a posteriori error estimates, which are used to control the adaptive finite element procedures in our numerical experiments. In Section 6, we present various numerical results for uniform and adaptive mesh refinement in space and time. Finally, we draw some conclusions in Section 7.

2 Space-time variational formulation and solvability results

We start with Ladyzhenskaya's space-time variational formulation of the parabolic initial-boundary value problem (1)–(3) in space-time Sobolev spaces, see [20] and the classical monographs [22, 21]: find $u \in H_0^{1,0}(Q) := \{v \in L_2(Q) : \nabla_x u \in [L_2(Q)]^d, u = 0 \text{ on } \Sigma\}$ such that

$$\begin{aligned}
 a(u, v) &:= \int_Q (-u \partial_t v + \nu \nabla_x u \cdot \nabla_x v) \, dQ = \\
 &\int_Q (f v + \mathbf{f} \cdot \nabla_x v) \, dQ + \int_\Omega u_0(x) v(x, 0) \, dx =: l(v), \quad \forall v \in H_{0,0}^{1,1}(Q),
 \end{aligned} \tag{4}$$

where $H_{0,0}^{1,1}(Q) := \{v \in L_2(Q) : \nabla_x u \in [L_2(Q)]^d, \partial_t u \in L_2(Q), u = 0 \text{ on } \Sigma, u = 0 \text{ on } \Sigma_T = \Omega \times \{T\}\}$. If $f \in L_{2,1}(Q) := \{v : Q \rightarrow \mathbb{R} : \int_0^T \|v(\cdot, t)\|_{L_2(\Omega)} dt < \infty\}$, $\mathbf{f} \in [L_2(Q)]^d$, $u_0 \in L_2(\Omega)$, and the coefficient $\nu \in L_\infty(Q)$ is uniformly bounded and positive, i.e., there exist positive constants $\underline{\nu}$ and $\bar{\nu}$ such that

$$\underline{\nu} \leq \nu(x, t) \leq \bar{\nu} \text{ for almost all } (x, t) \in Q, \quad (5)$$

then the space-time variational formulation (4) has a unique solution u that even belongs to the space $\dot{V}_2^{1,0}(Q) \subset H_0^{1,0}(Q)$; see [21], Chapter III, Paragraph 3, Theorem 3.2. In particular, this means that $\|u(\cdot, t)\|_{L_2(\Omega)}$ is continuous with respect to (wrt) t . Therefore, the initial condition makes sense in $L_2(\Omega)$. The same result can be obtained if we consider the solvability of (1)–(3) in the Bochner space $W(0, T) := \{v \in L_2(0, t; H_0^1(\Omega)) : \partial_t u \in L_2(0, t; H^{-1}(\Omega))\}$ of abstract functions u mapping the time interval $[0, T]$ to some Hilbert or Banach space $X(\Omega)$. Indeed, the parabolic initial-boundary value problem is uniquely solvable in $W(0, T)$, and $W(0, T)$ is continuously embedded into $C([0, T], L_2(\Omega))$; see, e.g., [25]. This view at parabolic initial-boundary value is closely connected with the so-called line variational formulations and the corresponding operator ordinary differential equations, and is the starting point for time-stepping methods.

If $f \in L_2(Q)$, $\mathbf{f} = \mathbf{0}$, $u_0 \in H_0^1(\Omega)$, and $\nu = 1$, then the solution $u \in H_0^{1,0}(Q)$ of (4) belongs to the space $H_0^{\Delta,1}(Q) = \{v \in H_0^1(Q) : \Delta_x v \in L_2(Q)\}$, and continuously depends on t in the norm of the space $H_0^1(\Omega)$; see [21], Chapter III, Paragraph 2, Theorem 2.1. This property is called maximal parabolic regularity. If $\nu = \nu(x, t)$ depends on x and t (non-autonomous case) possibly in discontinuous way (like in electrical machines, moving interfaces), then it is more involved to specify the most general conditions for ν such that maximal parabolic regularity happens, i.e. the solution $u \in H_0^{1,0}(Q)$ of (4) belongs to the space

$$H_0^{\mathcal{L},1}(Q) = \{v \in H_0^1(Q) : \mathcal{L}_x v := \operatorname{div}_x(\nu \nabla_x u) \in L_2(Q)\}.$$

Recently, Dier [12] proved maximal parabolic regularity provided that the corresponding elliptic form is of bounded variation. In our case, this means that ν is of bounded variation in t for almost all x . In the case of maximal parabolic regularity, we have $\partial_t u - \mathcal{L}_x u = f$ in $L_2(Q)$ that was the starting point for the derivation of consistent space-time finite element schemes in [24].

In general, for non-trivial $\mathbf{f} \in [L_2(Q)]^d$ (with jumps), we cannot expect maximal parabolic regularity. Motivated by applications, we assume that there exist a decomposition of the space-time cylinder $\bar{Q} = \bigcup_{i=1}^m \bar{Q}_i$ into m non-overlapping Lipschitz domains Q_1, \dots, Q_m such that the restriction of \mathbf{f} to Q_i belongs to $H(\operatorname{div}_x, Q_i)$ for all $i = 1, 2, \dots, m$, but may have jumps across the boundaries of these subdomains. Now, taking an arbitrary test function $v \in H_{0,0}^{1,1}(Q)$ with a compact support in Q_i , we immediately get

$$\int_{Q_i} (-u \partial_t v + \nu \nabla_x u \cdot \nabla_x v) dQ = \int_{Q_i} (f v + \mathbf{f} \cdot \nabla_x v) dQ. \quad (6)$$

from the space-time variational formulation (4). Rewriting the left-hand side and applying integration by parts on the right-hand side in (6), we obtain

$$\int_{Q_i} \begin{pmatrix} \nu \nabla_x u \\ -u \end{pmatrix} \cdot \nabla v \, dQ = \int_{Q_i} (f - \operatorname{div}_x \mathbf{f}) v \, dQ, \quad (7)$$

where $\nabla = (\nabla_x^\top \ \partial_t)^\top$ is the space-time gradient. This is nothing but the definition of the weak space-time divergence, i.e., we have

$$\operatorname{div} \begin{pmatrix} -\nu \nabla_x u \\ u \end{pmatrix} = f - \operatorname{div}_x \mathbf{f} \quad \text{in } L_2(Q_i). \quad (8)$$

The solution $u \in \mathring{V}_2^{1,0}(Q)$ of (4) also satisfies the integral identity; see [21], Chapter 3, identity (3.20) on p. 120,

$$\begin{aligned} & \int_Q (-u \partial_t v + \nu \nabla_x u \cdot \nabla_x v) \, dQ + \int_\Omega u(x, T) v(x, T) \, dx = \\ & \int_Q (f v + \mathbf{f} \cdot \nabla_x v) \, dQ + \int_\Omega u_0(x) v(x, 0) \, dx, \quad \forall v \in H_0^1(Q), \end{aligned} \quad (9)$$

from which one can derive the space-time flux relation

$$\begin{aligned} & \sum_{i=1}^m \int_{\partial Q_i} \begin{pmatrix} \nu \nabla_x u \\ -u \end{pmatrix} \cdot \begin{pmatrix} \mathbf{n}_x \\ n_t \end{pmatrix} v \, ds + \int_\Omega u(x, T) v(x, T) \, dx \\ & = \sum_{i=1}^m \int_{\partial Q_i} \mathbf{f} \cdot \mathbf{n}_x v \, ds + \int_\Omega u_0 v(x, 0) \, dx, \quad \forall v \in H_0^1(Q). \end{aligned} \quad (10)$$

Indeed, in (9), we can rewrite the integrals over Q as sum of integrals over Q_i . Then we have the variational identity

$$\begin{aligned} & \sum_{i=1}^m \int_{Q_i} \begin{pmatrix} \nu \nabla_x u \\ -u \end{pmatrix} \cdot \nabla v \, dQ + \int_\Omega u(x, T) v(x, T) \, dx \\ & = \sum_{i=1}^m \int_{Q_i} (f v + \mathbf{f} \cdot \nabla_x v) \, dQ + \int_\Omega u_0 v(x, 0) \, dx \end{aligned}$$

for all $v \in H_0^1(Q) = H_0^{1,1}(Q)$. Integrating by parts in the left-hand side and in the right-hand side gives the identity

$$\begin{aligned} & \sum_{i=1}^m \left(\int_{Q_i} \operatorname{div} \begin{pmatrix} -\nu \nabla_x u \\ u \end{pmatrix} v \, dQ + \int_{\partial Q_i} \begin{pmatrix} \nu \nabla_x u \\ -u \end{pmatrix} \cdot \begin{pmatrix} \mathbf{n}_x \\ n_t \end{pmatrix} v \, ds \right) \\ & \quad + \int_\Omega u(x, T) v(x, T) \, dx \\ & = \sum_{i=1}^m \left(\int_{Q_i} (f - \operatorname{div}_x \mathbf{f}) v \, dQ + \int_{\partial Q_i} \mathbf{f} \cdot \mathbf{n}_x v \, ds \right) + \int_\Omega u_0 v(x, 0) \, dx, \quad (11) \end{aligned}$$

that holds for all $v \in H_0^1(Q)$. We mention that the integral over ∂Q_i have to be understood as duality products on $H^{-1/2}(\partial Q_i) \times H^{1/2}(\partial Q_i)$. Using (8) in (11), we arrive at the space-time flux relation (10).

3 Space-time finite element methods

Next, we need a decomposition (triangulation) \mathcal{T}_h of Q into shape-regular finite elements K such that $\overline{Q} = \bigcup_{K \in \mathcal{T}_h} \overline{K}$ and $K \cap K' = \emptyset$ for all K and K' from \mathcal{T}_h with $K \neq K'$; see [4, 5, 8] for a precise definition of shape-regular triangulations. We assume that the triangulation is aligned with Q_i , i.e. $\overline{Q}_i = \bigcup_{K \in \mathcal{T}_{i,h}} \overline{K}$ can be represented by a subset $\mathcal{T}_{i,h}$ of the triangulation $\mathcal{T}_h = \bigcup_{i=1}^m \mathcal{T}_{i,h}$.

On the basis of the shape-regular triangulation \mathcal{T}_h , we define the space-time finite element space

$$V_{0h} = \{v \in C(\overline{Q}) : v(x_K(\cdot)) \in \mathbb{P}_p(\hat{K}), \forall K \in \mathcal{T}_h, v = 0 \text{ on } \overline{\Sigma}\} \quad (12)$$

as usual [4, 5, 8], where $x_K(\cdot)$ denotes the map from the reference element \hat{K} to the finite element $K \in \mathcal{T}_h$, and $\mathbb{P}_p(\hat{K})$ is the space of polynomials of the degree p on the reference element \hat{K} . The space-time finite elements space V_{0h} is obviously a finite dimensional subspace of the space $H_0^1(Q) \subset \dot{V}_2^{1,0}(Q)$. Let us denote the dimension of V_{0h} by N_h . For simplicity, throughout this paper and, in particular, in our numerical experiments in Section 6, we use affine-linear mappings $x_K(\cdot)$ and simplicial elements K .

Following [24], we first multiply (8), that is valid in $L_2(K)$ for all $K \in \mathcal{T}_h$ since the triangulation \mathcal{T}_h is align with Q_i , by a locally scaled upwind test function

$$v_{h,K}(x, t) := v_h(x, t) + \theta_K h_K \partial_t v_h(x, t), \quad v_h \in V_{0h},$$

then integrate over K , and finally sum over all $K \in \mathcal{T}_h$, giving the identity

$$\begin{aligned} & \sum_{K \in \mathcal{T}_h} \int_K \operatorname{div} \begin{pmatrix} -\nu \nabla_x u \\ u \end{pmatrix} (v_h + \theta_K h_K \partial_t v_h) \, dQ \\ &= \sum_{K \in \mathcal{T}_h} \int_K (f - \operatorname{div}_x \mathbf{f})(v_h + \theta_K h_K \partial_t v_h) \, dQ \end{aligned}$$

Integration by parts yields

$$\begin{aligned} & \sum_{K \in \mathcal{T}_h} \int_K \left[\nu \nabla_x u \cdot \nabla_x v_h - u \partial_t v_h + \theta_K h_K \operatorname{div} \begin{pmatrix} -\nu \nabla_x u \\ u \end{pmatrix} \partial_t v_h \, dQ \right] \\ & \quad + \sum_{K \in \mathcal{T}_h} \int_{\partial K} \begin{pmatrix} -\nu \nabla_x u \\ u \end{pmatrix} \cdot \begin{pmatrix} n_x \\ n_t \end{pmatrix} v_h \, ds \\ &= \sum_{K \in \mathcal{T}_h} \int_K [f v_h + \mathbf{f} \cdot \nabla_x v_h + \theta_K h_K f \partial_t v_h - \theta_K h_K \operatorname{div}_x \mathbf{f} \partial_t v_h] \, dQ \\ & \quad - \sum_{K \in \mathcal{T}_h} \int_{\partial K} \mathbf{f} \cdot n_x v_h \, ds \end{aligned}$$

Since the triangulation \mathcal{T}_h is aligned with the interfaces generated by the decomposition of Q into the space-time subdomains Q_1, Q_2, \dots, Q_m , the space-time

flux identity (10) is also valid if one replaces the subdomains Q_i by the finite elements K . Using (10) with Q_i replaced by K in the last identity, we immediately obtain the consistency relation

$$a_h(u, v_h) = l_h(v_h) \quad \forall v_h \in V_{0h}, \quad (13)$$

with

$$\begin{aligned} a_h(u, v_h) &:= \sum_{K \in \mathcal{T}_h} \int_K \left[\nu \nabla_x u \cdot \nabla_x v_h - u \partial_t v_h + \theta_K h_K \operatorname{div} \left(\begin{array}{c} -\nu \nabla_x u \\ u \end{array} \right) \partial_t v_h \right] dQ \\ &\quad + \int_{\Omega} u(x, T) v_h(x, T) dx, \\ l_h(v_h) &:= \sum_{K \in \mathcal{T}_h} \int_K [f v_h + \mathbf{f} \cdot \nabla_x v_h + \theta_K h_K f \partial_t v_h - \theta_K h_K \operatorname{div}_x(\mathbf{f}) \partial_t v_h] dQ \\ &\quad + \int_{\Omega} u_0(x) v_h(x, 0) dx. \end{aligned} \quad (14)$$

Therefore, we arrive at the following consistent space-time finite element scheme for solving the initial-boundary value problem (4): find $u_h \in V_{0h}$ such that

$$a_h(u_h, v_h) = l_h(v_h) \quad \forall v_h \in V_{0h}. \quad (15)$$

Subtracting the space-time finite element scheme (15) from the consistency relation (13), we get the Galerkin orthogonality relation

$$a_h(u - u_h, v_h) = 0 \quad \forall v_h \in V_{0h}, \quad (16)$$

that is crucial for deriving a priori discretization error estimates in the next section. We now show that the bilinear form $a_h(\cdot, \cdot)$ is coercive on V_{0h} with respect to the norm

$$\begin{aligned} \|v_h\|_h^2 &:= \sum_{K \in \mathcal{T}_h} \left[\|\nu^{1/2} \nabla_x v_h\|_{L_2(K)}^2 + \theta_K h_K \|\partial_t v_h\|_{L_2(K)}^2 \right] \\ &\quad + \|v_h(\cdot, T)\|_{L_2(\Omega)}^2 + \|v_h(\cdot, 0)\|_{L_2(\Omega)}^2. \end{aligned} \quad (17)$$

Lemma 1. *If θ_K is chosen sufficiently small, then there exist a positive constant μ_c such that*

$$a_h(v_h, v_h) \geq \mu_c \|v_h\|_h^2, \quad \forall v_h \in V_{0h}. \quad (18)$$

More precisely, if $\theta_K \leq h_K/c_{I,K,\nu}^2$ for all $K \in \mathcal{T}_h$, then μ_c can be chosen $1/2$, where $c_{I,K}(\nu)$ denotes the constant from the inverse inequality

$$\|\operatorname{div}_x(\nu \nabla_x v_h)\|_{L_2(K)} \leq c_{I,K,\nu} h_k^{-1} \|\nu^{1/2} \nabla_x v_h\|_{L_2(K)} \quad (19)$$

that holds for all $v_h \in V_{0h}$ and $K \in \mathcal{T}_h$; see [24].

Proof. For all $v_h \in V_{0h}$, we have the following representation of the bilinear form $a_h(v_h, v_h)$:

$$\begin{aligned}
a_h(v_h, v_h) &= \sum_{K \in \mathcal{T}_h} \int_K \left[|\nu^{1/2} \nabla_x v_h|^2 - \frac{1}{2} \partial_t v_h^2 + \theta_K h_K \operatorname{div} \begin{pmatrix} -\nu \nabla_x v_h \\ v_h \end{pmatrix} \partial_t v_h \right] dQ \\
&\quad + \int_{\Omega} |v_h(x, T)|^2 dx \\
&= \sum_{K \in \mathcal{T}_h} \int_K \left[|\nu^{1/2} \nabla_x v_h|^2 + \theta_K h_K |\partial_t v_h|^2 \right] dQ + \frac{1}{2} \int_{\Omega} |v_h(x, T)|^2 dx \\
&\quad + \frac{1}{2} \int_{\Omega} |v_h(x, 0)|^2 dx - \sum_{K \in \mathcal{T}_h} \theta_K h_K \int_K \operatorname{div}_x(\nu \nabla_x v_h) \partial_t v_h dQ \quad (20)
\end{aligned}$$

Estimating the last term by Cauchy's inequality, Young's inequality, and the inverse inequality (19), we immediately get

$$\begin{aligned}
a_h(v_h, v_h) &\geq \sum_{K \in \mathcal{T}_h} \left[\left(1 - \frac{\varepsilon \theta_K c_{I,K,\nu}^2}{2h_K}\right) \|\nu^{1/2} \nabla_x v_h\|_{L_2(K)}^2 + \left(1 - \frac{1}{2\varepsilon}\right) \theta_K h_K \|\partial_t v_h\|_{L_2(K)}^2 \right] \\
&\quad + \frac{1}{2} \|v_h(\cdot, T)\|_{L_2(\Omega)}^2 + \frac{1}{2} \|v_h(\cdot, 0)\|_{L_2(\Omega)}^2, \quad \forall v_h \in V_{0h},
\end{aligned}$$

from which (1) follows for $\varepsilon = 1$ and $\theta_K \leq h_K/c_{I,K,\nu}^2$ for all $K \in \mathcal{T}_h$. \square

Remark 2. For the special case that $p = 1$ (linear shape functions) and $\nu = \nu_K = \text{const}$ for all $K \in \mathcal{T}_h$, the last term in (20) vanishes since $\operatorname{div}_x(\nu \nabla_x v_h) = \nu_K \Delta_x v_h = 0$ on K . Therefore, we have

$$\begin{aligned}
a_h(v_h, v_h) &= \sum_{K \in \mathcal{T}_h} \int_K \left[|\nu^{1/2} \nabla_x v_h|^2 + \theta_K h_K |\partial_t v_h|^2 \right] dQ + \frac{1}{2} \int_{\Omega} |v_h(x, T)|^2 dx \\
&\quad + \frac{1}{2} \int_{\Omega} |v_h(x, 0)|^2 dx =: \|v_h\|_h^2, \quad \forall v_h \in V_{0h}, \quad (21)
\end{aligned}$$

i.e. the bilinear form $a_h(\cdot, \cdot)$ is coercive on V_{0h} wrt the norm $\|\cdot\|_h$ with the constant $\mu_c = 1$.

The coercivity of the bilinear form $a_h(\cdot, \cdot)$ on V_{0h} yields uniqueness, and, in the finite-dimensional case, uniqueness implies existence. Thus, the space-time finite element scheme (15) has a unique solution $u_h \in V_{0h}$ that can be found by solving one linear system of algebraic equations. Once the basis is chosen, the space-time finite element scheme (15) is nothing but one system of linear algebraic equations. Indeed, let $\{p^{(j)} : j = 1, \dots, N_h\}$ be the finite element nodal basis of V_{0h} , i.e., $V_{0h} = \operatorname{span}\{p^{(1)}, \dots, p^{(N_h)}\}$, where N_h is the number of all space-time unknowns (dofs). Then we can express the approximate solution u_h in terms of this basis, i.e., $u_h(x, t) = \sum_{j=1}^{N_h} u_j p^{(j)}(x, t)$. Inserting this ansatz into (15) and testing with $p^{(i)}$, we get the linear system

$$K_h \underline{u}_h = \underline{f}_h, \quad (22)$$

for determining the unknown coefficient vector $\underline{u}_h = (u_j)_{j=1,\dots,N_h} \in \mathbb{R}^{N_h}$, where $K_h = (a_h(p^{(j)}, p^{(i)}))_{i,j=1,\dots,N_h}$ and $\underline{f}_h = (f_h(p^{(i)}))_{i=1,\dots,N_h}$. The system matrix K_h is non-symmetric, but positive definite due to Lemma 1.

4 A priori error estimates

We now introduce the norm

$$\begin{aligned} \|u\|_{h,*}^2 := & \sum_{K \in \mathcal{T}_h} \left[\|\nu^{1/2} \nabla_x u\|_{L_2(K)}^2 + (\theta_K h_K)^{-1} \|u\|_{L_2(K)}^2 \right. \\ & \left. + \theta_K h_K \|\operatorname{div} \begin{pmatrix} -\nu \nabla_x u \\ u \end{pmatrix}\|_{L_2(K)}^2 \right] + \|u(\cdot, T)\|_{L_2(\Omega)}^2 \end{aligned}$$

that is defined on $V_{0h,*} = H_0^{\mathcal{L}}(\mathcal{Q}) + V_{0h}$ to which the solution u and the discretization error $u - u_h$ belong. The solution space $H_0^{\mathcal{L}}(\mathcal{Q})$ can be chosen as $\{v \in H_0^{1,0}(\mathcal{Q}) : \mathcal{L}u := \operatorname{div}(-\nu \nabla_x u, u) \in L_2(Q_i), i = 1, \dots, m\}$.

Lemma 3. *The bilinear form (14) is bounded on $V_{0h,*} \times V_{0h}$, i.e.,*

$$|a_h(u, v_h)| \leq \mu_b \|u\|_{h,*} \|v_h\|_h, \quad \forall u \in V_{0h,*}, v_h \in V_{0h} \quad (23)$$

with $\mu_b = 1$.

Proof. Using Cauchy's inequalities, we immediately get

$$\begin{aligned} a_h(u, v_h) &= \sum_{K \in \mathcal{T}_h} \int_K \nu \nabla_x u \cdot \nabla_x v_h - u \partial_t v_h + \theta_K h_K \operatorname{div} \begin{pmatrix} -\nu \nabla_x u \\ u \end{pmatrix} \partial_t v_h \, dQ \\ &\quad + \int_{\Omega} u(x, T) v_h(x, T) \, dx \\ &\leq \sum_{K \in \mathcal{T}_h} \left[\left(\|\nu^{1/2} \nabla_x u\|_{L_2(K)}^2 \right)^{1/2} \left(\|\nu^{1/2} \nabla_x v_h\|_{L_2(K)}^2 \right)^{1/2} \right. \\ &\quad + \left((\theta_K h_K)^{-1} \|u\|_{L_2(K)}^2 \right)^{1/2} \left(\theta_K h_K \|\partial_t v_h\|_{L_2(K)}^2 \right)^{1/2} \\ &\quad + \left(\theta_K h_K \|\operatorname{div} \begin{pmatrix} -\nu \nabla_x u \\ u \end{pmatrix}\|_{L_2(K)}^2 \right)^{1/2} \left(\theta_K h_K \|\partial_t v_h\|_{L_2(K)}^2 \right)^{1/2} \left. \right] \\ &\quad + \left(\|u(\cdot, T)\|_{L_2(\Omega)}^2 \right)^{1/2} \left(\|v_h(\cdot, T)\|_{L_2(\Omega)}^2 \right)^{1/2} \\ &\leq \mu_b \|u\|_{h,*} \|v_h\|_h \end{aligned}$$

with $\mu_b = 1$. □

The Galerkin orthogonality (16) together with the coercivity (18) and the generalized boundedness (23) of the bilinear form $a_h(\cdot, \cdot)$ immediately yield a best-approximation (Céa-like) discretization error estimate in the corresponding norms.

Lemma 4. *Let $u \in H_0^{\mathcal{L}}(\mathcal{Q})$ and $u_h \in V_{0h}$ be the solutions of the parabolic IBVP (4) and the space-time finite element scheme (15), respectively, and let the assumptions of Lemma 1 (coercivity) Lemma 3 (boundedness) hold. Then the discretization error estimate*

$$\|u - u_h\|_h \leq \inf_{v_h \in V_{0h}} \left(\|u - v_h\|_h + \frac{\mu_b}{\mu_c} \|u - v_h\|_{h,*} \right) \quad (24)$$

holds.

Proof. Using (18), (16), and (23), we immediately get the estimates

$$\mu_c \|v_h - u_h\|_h^2 \leq a_h(v_h - u_h, v_h - u_h) = a_h(u - u_h, v_h - u_h) \leq \mu_b \|u - u_h\|_h \|u - v_h\|_{h,*}$$

for any $v_h \in V_{0h}$, from which (24) follows by triangle inequality. \square

In order to obtain a convergence rate estimate from (24), we have to insert a suitable interpolation or quasi-interpolation $I_h^p(u) \in V_{0h}$ of the solution u into the infimum. If u is sufficiently smooth, then we can use the nodal Lagrange interpolation that leads to completely local estimates. More precisely, let $u \in H_0^{\mathcal{L}}(\mathcal{Q}) \cap H^k(Q) \cap H^l(\mathcal{T}_h)$ with some $l \geq k > (d+1)/2$. Since in this case $H^k(Q) \subset C(\bar{Q})$, the nodal Lagrange interpolation is well defined. Then the standard finite element interpolation error estimates (see, e.g., [5, Theorem 4.4.4] or [8, Theorem 3.1.6]) and the best-approximation error estimate (24) lead to the a priori discretization error estimate

$$\|u - u_h\|_h \leq c \left(\sum_{K \in \mathcal{T}_h} h_K^{2(s-1)} |u|_{H^s(K)}^2 \right)^{1/2} \quad (25)$$

with $s = \min\{l, p+1\}$ and some generic positive constant c ; see [24, Theorem 13.3]. If the nodal Lagrange interpolation is not well defined due to the low regularity of the solution u , we can make use of the quasi-interpolators proposed by Clément [10] or Scott and Zhang [33]. Let $v \in H^k(Q)$, with some $k > 1$. Then, for instance, the Scott-Zhang quasi-interpolation operator $I_h^{SZ} : H^1(Q) \rightarrow V_{0h}$ provides the local interpolation error estimate

$$\|v - I_h^{SZ} v\|_{H^m(K)} \leq ch_K^{s-m} |v|_{H^s(S_K)}, \quad m = 0, 1, \quad (26)$$

where $s = \min\{k, p+1\}$, c is again a generic positive constant, and $S_K := \{K' \in \mathcal{T}_h : \bar{K} \cap \bar{K}' \neq \emptyset\}$ denotes the neighborhood of the simplex $K \in \mathcal{T}_h$; see monograph [5, (4.8.10)] or the original paper [33], and space interpolation results [3, 15].

Theorem 5. *Beside the assumptions imposed on the data ν , f , \mathbf{f} and Q , and the triangulation \mathcal{T}_h , we assume that the solution u of the space-time variational problem (4) belongs to $H_0^{\mathcal{L}}(\mathcal{Q}) \cap H^k(Q)$, $(d+1)/2 \geq k > 1$, and $\nu \nabla_x(u) \in$*

$(H^{k-1}(K))^d$ for all $K \in \mathcal{T}_h$. Furthermore, let the assumptions of Lemma 4 be fulfilled. Then the a priori discretization error estimate

$$\|u - u_h\|_h^2 \leq c \sum_{K \in \mathcal{T}_h} \left[h_K^{2(s-1)} (|u|_{H^s(S_K)}^2 + |\nu \nabla_x u|_{H^{s-1}(K)}^2) + h_K^2 \|\operatorname{div}_x(\nu \nabla_x u)\|_{L_2(K)}^2 \right] \quad (27)$$

holds, with $s = \min\{k, p+1\} = k \leq (d+1)/2$ for $d = 1, 2, 3$ and a positive generic constant c .

Proof. Inserting $v_h = I_h^{SZ} u \in V_{0h}$ into the infimum of the right-hand side of the best-approximation error estimate (24), we immediately get

$$\begin{aligned} \|u - u_h\|_h^2 &\leq \left(\|u - I_h^{SZ} u\|_h + \frac{\mu_b^2}{\mu_c^2} \|u - I_h^{SZ} u\|_{h,*} \right)^2 \\ &\leq 2\|e_h\|_h^2 + 2\frac{\mu_b^2}{\mu_c^2} \|e_h\|_{h,*}^2 \\ &\leq \sum_{K \in \mathcal{T}_h} \left[2\left(1 + \frac{\mu_b^2}{\mu_c^2}\right) \|\nu^{1/2} \nabla_x e_h\|_{L_2(K)}^2 + 2\theta_K h_K \|\partial_t e_h\|_{L_2(K)}^2 \right. \\ &\quad \left. + 2\frac{\mu_b^2}{\mu_c^2} (\theta_K h_K)^{-1} \|e_h\|_{L_2(K)}^2 + 2\frac{\mu_b^2}{\mu_c^2} \theta_K h_K \|\operatorname{div} \begin{pmatrix} -\nu \nabla_x e_h \\ e_h \end{pmatrix}\|_{L_2(K)}^2 \right] \\ &\quad + 2\left(1 + \frac{\mu_b^2}{\mu_c^2}\right) \|e_h(\cdot, T)\|_{L_2(\Omega)}^2 + 2\|e_h(\cdot, 0)\|_{L_2(\Omega)}^2, \end{aligned} \quad (28)$$

where $e_h = u - I_h^{SZ} u$ denotes the interpolation error. The first three terms in the sum can directly be estimated by means of the local interpolation error estimate (26). The fourth term needs special treatment. Inserting and subtracting the average

$$I_h^0 q(x) = \frac{1}{|K|} \int_K q(y) dy \in \mathbb{R}^{d+1} \text{ for } x \in K \quad (29)$$

of the space-time flux $q = (-\nu(\nabla_x u)^T, u)^T$ over $K \in \mathcal{T}_h$ and using the inverse inequalities $\|\operatorname{div}_x(c_h + \nu \nabla_x v_h)\|_{L_2(K)} \leq ch_K^{-1} \|c_h + \nu \nabla_x v_h\|_{L_2(K)}$ for all $(c_h, v_h) \in \mathbb{R}^d \times V_{0h}$ and $\|\partial_t(c_h - v_h)\|_{L_2(K)} \leq ch_K^{-1} \|c_h - v_h\|_{L_2(K)}$ for all $(c_h, v_h) \in \mathbb{R} \times V_{0h}$, we can estimate this term as follows:

$$\begin{aligned} \|\operatorname{div} \begin{pmatrix} -\nu \nabla_x e_h \\ e_h \end{pmatrix}\|_{L_2(K)} &= \|\operatorname{div}(q - I_h^0 q + I_h^0 q - \begin{pmatrix} -\nu \nabla_x(I_h^{SZ} u) \\ I_h^{SZ} u \end{pmatrix})\|_{L_2(K)} \\ &\leq \|\operatorname{div} q\|_{L_2(K)} + \|\operatorname{div}(I_h^0 q - \begin{pmatrix} -\nu \nabla_x(I_h^{SZ} u) \\ I_h^{SZ} u \end{pmatrix})\|_{L_2(K)} \\ &\leq \|\operatorname{div} q\|_{L_2(K)} + ch_K^{-1} \|I_h^0 q - \begin{pmatrix} -\nu \nabla_x(I_h^{SZ} u) \\ I_h^{SZ} u \end{pmatrix}\|_{L_2(K)}. \end{aligned}$$

Now, the last term can be estimated by means of the local approximation properties of I_h^0 and I_h^{SZ} . Indeed, inserting and subtracting q in the last term of the

above estimate, we get

$$\begin{aligned} \|I_h^0 q - \left(\begin{array}{c} -\nu \nabla_x (I_h^{SZ} u) \\ I_h^{SZ} u \end{array} \right)\|_{L_2(K)}^2 &\leq 2\|I_h^0 q - q\|_{L_2(K)}^2 + 2\|q - \left(\begin{array}{c} -\nu \nabla_x (I_h^{SZ} u) \\ I_h^{SZ} u \end{array} \right)\|_{L_2(K)}^2 \\ &\leq c \left(h_K^{2(s-1)} |\nu \nabla_x(u)|_{H^{s-1}(K)}^2 + h_K^2 |u|_{H^1(K)}^2 + h_K^{2(s-1)} |u|_{H^s(S_K)}^2 + h_K^{2s} |u|_{H^s(S_K)}^2 \right), \end{aligned}$$

where we have used the Poincaré inequality for estimating the first term and (26) for the second term. Finally, we have to estimate the last two terms in (28). The trace theorem and the local interpolation error estimate (26) yield the estimates

$$\|e_h(\cdot, T)\|_{L_2(\Omega)}^2 \leq c \|e_h\|_{H^1(Q)}^2 \leq c \sum_{K \in \mathcal{T}_h} \|e_h\|_{H^1(K)}^2 \leq c \sum_{K \in \mathcal{T}_h} h_K^{2(s-1)} |u|_{H^s(S_K)}^2$$

that is obviously also valid for the last term $\|e_h(\cdot, 0)\|_{L_2(\Omega)}^2$ in (28). Combining these estimates, we arrive at (27). \square

5 A posteriori error estimates and adaptivity

In contrast to elliptic boundary value problems, there are not so many results on space-time a posteriori error estimates and simultaneous space-time adaptivity driven by the corresponding error indicators for finite element schemes on unstructured simplicial meshes that treat time t as just another variable, say, x_{d+1} , like in this paper; cf. also survey paper [36]. As in the elliptic case, Steinbach and Yang [35] have recently proposed to use the local residual error indicator

$$\eta_K := \left(h_K^2 \|R_h(u_h)\|_{L_2(K)}^2 + h_K \|J_h(u_h)\|_{L_2(\partial K)}^2 \right)^{1/2} \quad (30)$$

for driving the adaptivity, where u_h is the space-time finite element solution, $R_h(u_h) := f + \operatorname{div}_x(\nu \nabla_x u_h) - \partial_t u_h$ denotes the residual on $K \in \mathcal{T}_h$, $J_h(u_h) := [\nu \nabla_x u_h]_e$ represents the jump of the space flux across one face $e \subset \partial K$ of the boundary ∂K of an element $K \in \mathcal{T}_h$. Here, we assume that there are no distributional sources, i.e., $\mathbf{f} = \mathbf{0}$. While one has complete theoretical control on the adaptive process (reliability, efficiency, convergence, optimality) in the elliptic case, see [7] and the references therein, similar theoretical results are not available for adaptive processes based on the residual error indicator (30). Even the reliability is not shown theoretically, although the numerical results presented in [35, 36] show the same behavior as in the elliptic case.

Repin proposed functional a posteriori discretization error estimates for the instationary heat equation in [30], see also Repin's monograph [31][Section 9.3, pp. 229–242]. Repin's first form of the error majorant

$$\begin{aligned} \overline{\mathfrak{M}}_1^2(\beta, \delta, v, \mathbf{y}) &:= \int_{\Omega} |v(x, 0) - u_0(x)|^2 dx \\ &+ \frac{1}{\delta} \int_Q \left[(1 + \beta) |\mathbf{f} + \mathbf{y} - \nu \nabla_x v|^2 + c_{F\Omega}^2 \left(1 + \frac{1}{\beta}\right) |f - \partial_t v + \operatorname{div}_x \mathbf{y}|^2 \right] dQ \end{aligned}$$

provides a guaranteed upper bound of the error $u - v$ with respect to the norm

$$\|u - v\|_{(1,2-\delta)}^2 := (2 - \delta) \|\nabla_x(u - v)\|_{L_2(Q)}^2 + \|u - v\|_{L_2(\Sigma_T)}^2 \leq \overline{\mathfrak{M}}_1^2(\beta, \delta, v, \mathbf{y}) \quad (31)$$

for any approximation $v \in H_0^1(Q)$ to the solution u of (4), for any flux $\mathbf{y} \in H(\operatorname{div}_x, Q) := \{\mathbf{y} \in (L_2(Q))^d : \operatorname{div}_x(\mathbf{y}) \in L_2(Q)\}$, and for any weight function $\beta \in L_\mu^\infty(0, T) := \{\beta \in L^\infty(0, T) : \beta(t) \geq \mu \text{ for almost all } t \in (0, T)\}$. Here $\delta \in (0, 2]$ and $\mu \in (0, 1)$ are fixed parameters, and $c_{F\Omega}$ is the Friedrichs constant for the space domain Ω . Estimate (31) is proven in Theorem 9.6 from [31] for the case $\mathbf{f} = \mathbf{0}$, but the proof remains unchanged in the presence of distributional sources. In particular, we can choose our finite element solution $u_h \in V_{0h} \subset H_0^1(Q)$ as v in (31). The parameter $\delta \in (0, 2]$ can be chosen to weight the two parts of the norm $\|\cdot\|_{(1,2-\delta)}$, e.g., the choice $\delta = 1$ equilibrates both parts, whereas the choice $\delta = 2$ provides a L_2 error estimate at the final time $t = T$. In order to compute an upper bound on the discretization error $u - u_h$ via estimate (31), we have to choose appropriate fluxes $\mathbf{y} \in H(\operatorname{div}_x, Q)$ and weight functions $\beta \in L_\mu^\infty(0, T)$. We cannot choose $\mathbf{y} = \nu \nabla_x u_h - \mathbf{f}$ since the finite element flux $\nu \nabla_x u_h$ does not belong to $H(\operatorname{div}_x, Q)$ in general. Thus, we have to postprocess the finite element flux in such a way that the postprocessed finite element flux $P_h(\nu \nabla_x u_h)$ belongs to some $Y_h \subset H(\operatorname{div}_x, Q)$. In our numerical experiments in Section 6, we simply average the finite element flux in the vertices; see e.g. [37, 38]. Then one can calculate β from the minimization of the majorant. If we choose β as a positive constant, then we get

$$\beta^{(0)} = c_{F\Omega} \overline{\mathfrak{M}}_{eq}(u_h, \mathbf{y}_h^{(0)}) / \overline{\mathfrak{M}}_{flux}(u_h, \mathbf{y}_h^{(0)}) \quad (32)$$

where $\mathbf{y}_h^{(0)} = P_h(\nu \nabla_x u_h) - \mathbf{f}$, $\overline{\mathfrak{M}}_{eq}(u_h, \mathbf{y}_h^{(0)}) = \int_Q |f - \partial_t u_h + \operatorname{div}_x \mathbf{y}_h^{(0)}|^2 dQ$, and $\overline{\mathfrak{M}}_{flux}(u_h, \mathbf{y}_h^{(0)}) = \int_Q |\mathbf{f} + \mathbf{y}_h^{(0)} - \nu \nabla_x u_h|^2 dQ$. If one is not satisfied with the bound $\overline{\mathfrak{M}}_1^2(\beta^{(0)}, \delta, u_h, \mathbf{y}_h^{(0)})$, then one can start an alternating minimization of the majorant $\overline{\mathfrak{M}}_1^2(\beta, \delta, u_h, \mathbf{y}_h)$ with respect to \mathbf{y}_h and β , where one has to solve the auxiliary problem: find $\mathbf{y}_h^{(k+1)} \in Y_h$ such that

$$\mathbf{A}_k(\mathbf{y}_h^{(k+1)}, \mathbf{w}_h) = \mathbf{F}_k(\mathbf{w}_h) \quad \forall \mathbf{w}_h \in Y_h \quad (33)$$

for improving the fluxes followed by calculating improved weights $\beta^{(k+1)}$ via formula (32), where $Y_h \subset H(\operatorname{div}_x, Q)$ is a suitable finite element space for the fluxes,

$$\begin{aligned} \mathbf{A}_k(\mathbf{y}_h, \mathbf{w}_h) &:= \sum_{K \in \mathcal{T}_h} \int_K \left((1 + \beta^{(k)}) \mathbf{y}_h \cdot \mathbf{w}_h \right. \\ &\quad \left. + c_{F\Omega}^2 (1 + 1/\beta^{(k)}) \operatorname{div}_x(\mathbf{y}_h) \operatorname{div}_x(\mathbf{w}_h) \right) dQ, \\ \mathbf{F}_k(\mathbf{w}_h) &:= \sum_{K \in \mathcal{T}_h} \int_K \left((1 + \beta^{(k)}) (\nu \nabla_x u_h - \mathbf{f}) \cdot \mathbf{w}_h \right. \\ &\quad \left. - c_{F\Omega}^2 (1 + 1/\beta^{(k)}) (f - \partial_t u_h) \operatorname{div}_x(\mathbf{w}_h) \right) dQ, \end{aligned}$$

In the numerical experiments presented in Section 6, we choose $\delta = 1$, and, as already mentioned above, $v = u_h$. Furthermore, we use the nodal averaging procedure to post-process the finite element flux $\nu \nabla_x u_h$. We use the finite element space $Y_h = (V_h)^d \subset (H^1(Q))^d \subset H(\operatorname{div}_x, Q)$ for the fluxes. Note that this choice might be too restrictive since it excludes fluxes that are only continuous in their normal component. We apply one iteration of the alternating minimization described above, i.e., we have to solve the auxiliary problem (33) once, which is symmetric and positive definite. Hence, we can apply a few iterations of the (preconditioned) Conjugate Gradient (CG) method, where the post-processed flux $\mathbf{y}_h^{(0)}$ is used as initial guess. We then use the first part of the majorant

$$\eta_K(u_h) = \|\mathbf{f} + \mathbf{y}_h^{(1)} - \nu \nabla_x u_h\|_{L_2(K)},$$

as an error indicator, where $\mathbf{y}_h^{(1)}$ results from the improvement of $\mathbf{y}_h^{(0)}$ by a few CG iterations. We proceed by using Dörfler marking [13] as a marking strategy, i.e., we determine a set $\mathcal{M} \subseteq \mathcal{T}_h$ of (almost) minimal cardinality such that

$$\Xi \eta(u_h)^2 \leq \sum_{K \in \mathcal{M}} \eta_K(u_h)^2,$$

with a suitable bulk parameter $\Xi \in (0, 1]$. In particular, we use the implementation recently proposed by Pfeiler et al. [28], which is straightforward to parallelize. We will also survey the efficiency index of the a posteriori error estimator, that is defined as

$$\mathbf{I}_{\text{eff}}^2 = \frac{\sum_{K \in \mathcal{T}_h} \eta_K(u_h)^2}{\|u - u_h\|_h^2},$$

with the exact solution u and its finite element approximation u_h .

6 Numerical results

In this section, we present the results of an extensive set of numerical experiments. We realized the space-time FEM in our C++ code “SpTmFEM”, using the fully parallelized finite element library MFEM [27], where we implemented arbitrary-order finite elements in 4D. The large linear systems arising from the discretized variational problem are solved by means of a flexible Generalized Minimal Residual (GMRES) method [32], preconditioned by an algebraic multigrid V-cycle. In particular, we use the *BoomerAMG*, provided by the solver library *hypr*¹. We start the iterative solver with the initial guess zero, and stop once the initial residual is reduced by a factor of 10^{-8} . However, especially in an adaptive procedure, it may be better to interpolate the solution from the previous refinement level to the current one and use it as an initial guess for the iterative solver. In addition, we relax the stopping criterion, i.e., we stop

¹<https://computing.llnl.gov/projects/hypr-scalable-linear-solvers-multigrid-methods>

once the initial residual is reduced by a factor of e.g. 10^{-2} . This approach is sometimes referred to as *Nested Iterations (NI)*.

All numerical experiments were performed on the distributed memory cluster **Quartz**², located at the Lawrence Livermore National Laboratory.

6.1 Moving peak

For our first example, we consider the four dimensional hyper-cube $Q = (0, 1)^4$ as space-time cylinder, the diffusion coefficient $\nu \equiv 1$, and we use the manufactured solution

$$u(x, t) = \prod_{i=1}^3 (x_i^2 - x_i)(t^2 - t)e^{-100((x_1-t)^2+(x_2-t)^2+(x_3-t)^2)}.$$

We then compute the right-hand side and boundary data accordingly. This solution is very smooth. Thus, we would expect optimal convergence rates for uniform mesh refinement. However, the solution is also very localized and has steep gradients. In order to recover the optimal convergence rate quickly, we will apply adaptive mesh refinement based on the error estimator from the previous section. Moreover, we compare the efficiency index I_{eff} of the functional error estimator with that of the residual-based error indicator proposed by Steinbach and Yang [36]. In Figure 1, we present the relative error in the energy norm (17), using both uniform and adaptive refinement, as well as different polynomial degrees for the finite element shape functions. We can observe the expected behavior, i.e., even a sufficiently uniformly refined mesh results in an (almost) optimal convergence rate wrt the polynomial degree. However, adaptive refinement results in optimal convergence rates, and, moreover, reduces the number of dofs needed to obtain an error below a certain threshold, e.g., for $p = 3$, a relative error below 1% needs only 4 742 845 adaptive space-time dofs, compared to more than 81 044 161 dofs using uniform refinement. In the left of Figure 2, we plot the efficiency indices of the functional estimator and the residual indicator for different polynomial degrees. For the functional estimator, we observe efficiency indices $I_{\text{eff}} \sim 1.4$, independently of the polynomial degree p . The efficiency index of the residual indicator depends on p . For $p = 1$, we observe efficiency indices around 1 whereas the efficiency indices are much worse for higher polynomial degrees p .

6.2 Circular Arc Scan Track

The next example was introduced in [6] as a simplified model for simulating in-stationary heat transfer in additive manufacturing processes. We again have a very localized right-hand side, but this time we do not know the exact solution. Hence, we will compare the finite element solutions produced by adaptive refinement with a finite element solution obtained on a very fine, uniformly refined

²<https://hpc.llnl.gov/hardware/platforms/Quartz>

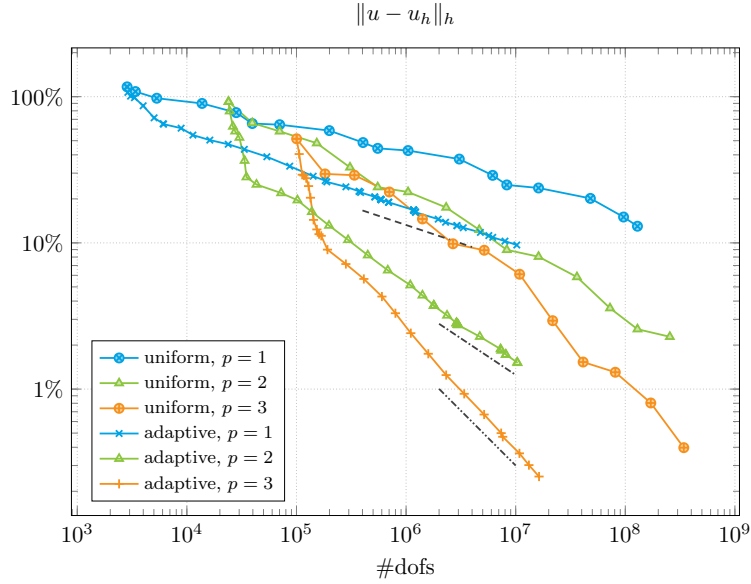


Figure 1: Example 6.1: Convergence rates of uniform and adaptive refinements, using the functional estimator, for $d = 3$ with marking threshold $\Xi = 0.25$.

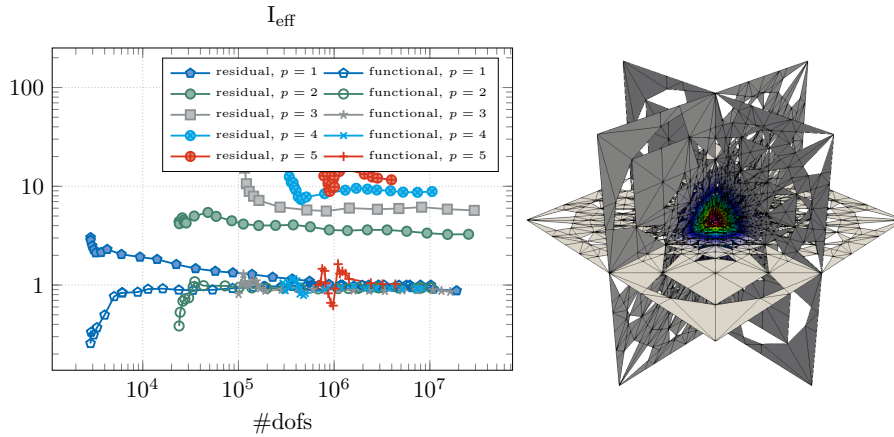


Figure 2: Example 6.1: Efficiency indices (lower left); and the mesh after 20 adaptive refinements, cut at $t = 0.5$ (lower right); for $d = 3$, and $\Xi = 0.25$.

mesh. We consider the space-time cylinder $Q = (0, 10)^2 \times (0, 5)$, the thermal conductivity coefficient $\nu \equiv 1$, the right hand side

$$f(x, t) = 2.97 \times 10^5 \exp(-100 ((x_1 - \bar{x}_1(t))^2 + (x_2 - \bar{x}_2(t))^2)),$$

with $(\bar{x}_1(t), \bar{x}_2(t)) = (5(1 + \cos(\pi(5+2t)/20)), 3 + 5 \sin(\pi(5+2t)/20))$, the initial condition $u_0 \equiv 20$ on Σ_0 , and the Neumann boundary condition $\nu \nabla_x u \cdot \vec{n}_x = 0$ on Σ ; see also [6]. In the left plot of Figure 3, we present the convergence rates in the energy-norm $\|\cdot\|_h$, for different combinations of polynomial degree p and a posteriori error indicators/estimators. The stagnation at the end of each line is due to the local mesh resolution of the adaptively refined mesh that is getting smaller than the mesh resolution of the reference solution. In terms of convergence rates, the functional error estimator gives clearly better rates for linear elements, whereas the rates for quadratic and cubic elements are almost indistinguishable. However, when we compare the efficiency index I_{eff} , we observe a notable difference. While $I_{\text{eff}} \sim 1$ for the functional estimator independently of p , the efficiency index for the residual indicator is also close to 1 for linear elements, but much worse when we increase the polynomial degree. In

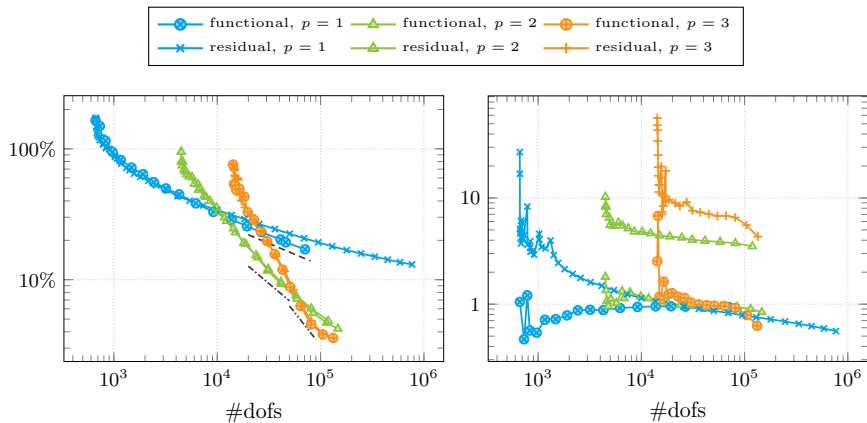


Figure 3: Example 6.2: Convergence rates in the energy norm (left); Efficiency indices I_{eff} (right); for different polynomial degrees p , and parameter $\Xi = 0.25$.

Figure 4, we present cuts through the space-time mesh, which was obtained after 10 adaptive refinements, using the functional estimator with bulk parameter $\Xi = 0.25$. We can clearly observe that the mesh refinement follows the source. Moreover, the middle mesh seems to show triangles with very sharp angles, but which is due to the cut through the completely unstructured space-time mesh.

6.3 Non-autonomous Kellogg's interface problem

We choose the space-time cylinder $Q = (-1, 1)^2 \times (0, 1)$, and the discontinuous diffusion coefficient

$$\nu(x, t) = \begin{cases} \nu_{13}(t), & (x, t) \in Q_1 \cup Q_3, \\ \nu_{24}(t), & (x, t) \in Q_2 \cup Q_4, \end{cases}$$

where $\nu_{13}(t) = Rt + (1-t)$ and $\nu_{24}(t) = (1-t)/R + t$, with $R = 161.4476387975884$, and $\bar{Q} = \bigcup_{i=1}^4 \bar{Q}_i$, $Q_i = \Omega_i \times (0, 1)$, $i = 1, \dots, 4$, and $\Omega_1 = (0, 1)^2$, $\Omega_2 =$

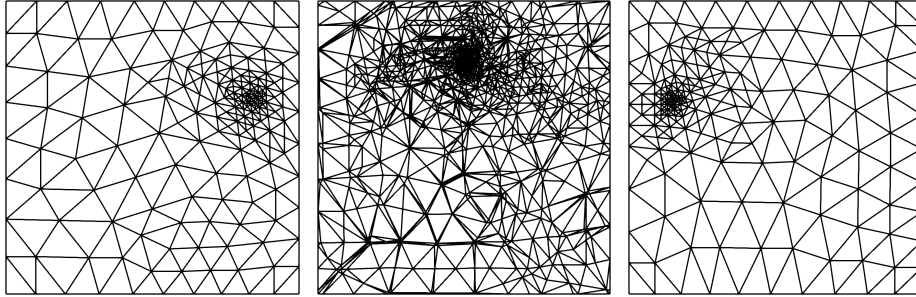


Figure 4: Example 6.2: Cuts through the space-time mesh, after 10 adaptive refinements, from left to right, at times $t = 0$, $t = 2.5$, and $t = 5$.

$(-1, 0) \times (0, 1)$, $\Omega_3 = (-1, 0)^2$ and $\Omega_4 = (0, 1) \times (-1, 0)$. We use the manufactured solution

$$u(x, t) = r(x)^\gamma \mu(\varphi(x)) t,$$

with

$$\mu(\varphi) := \begin{cases} \cos((\frac{\pi}{2} - \sigma)\gamma) \cos((\varphi - \frac{\pi}{2} + \rho)\gamma), & 0 \leq \varphi \leq \frac{\pi}{2}, \\ \cos(\gamma\rho) \cos((\varphi - \pi + \sigma)\gamma), & \frac{\pi}{2} \leq \varphi \leq \pi, \\ \cos(\gamma\sigma) \cos((\varphi - \pi - \rho)\gamma), & \pi \leq \varphi \leq \frac{3\pi}{2}, \\ \cos((\frac{\pi}{2} - \rho)\gamma) \cos((\varphi - 3\frac{\pi}{2} - \sigma)\gamma), & \text{else,} \end{cases}$$

where $\gamma = 0.1$, $\rho = \pi/4$, $\sigma = -19\pi/4$, and (r, φ) represents the polar coordinates of the spatial variable x . The parameters R , ρ and σ are related via a nonlinear system of equations, which can be found in [19], and determine the regularity of the function u . The above choice results in $u \in H^{1+\gamma}(Q_i)$, i.e., $u \in H^{1.1}(Q_i)$. According to the discretization error estimate (26), we cannot expect better convergence rates than $\|u - u_h\|_h \sim \mathcal{O}(h^\gamma)$ for uniform mesh refinement, regardless of the chosen polynomial degree p . This behavior can be observed in Figure 5, where the energy errors for uniform refinement have the same rate for $p = 1, \dots, 3$, i.e. $\sim \mathcal{O}(h^{0.1})$, up to a constant factor. When we compare the error rates for the adaptive refinements, we observe an improved rate of approximately $\mathcal{O}(N_h^{-0.3/3})$, which is still not (quasi-)optimal. One reason for this behavior might be the anisotropic nature of the singularity, which is located at the origin for all times t . Some preliminary tests with hexahedral elements and anisotropic refinement indeed recovered the optimal rates, and the refinements were mostly concentrated in the spatial directions. In the left part of Figure 6, we present the efficiency indices of the residual indicator and the functional estimator for different polynomial degrees p . In order to keep the plot readable, we cut off all values below 0.01 for the linear case of the residual indicator. For this example, the residual indicator yields efficiency indices $I_{\text{eff}} \sim 1.5$ for $p = 2$ and $I_{\text{eff}} \sim 3$ for $p = 3$, whereas the functional estimator gives efficiency indices $I_{\text{eff}} \sim 10 - 20$, for all tested p . This is also resembled in the convergence rates, where we obtain slightly better results, in both value and rate, for the residual indicator with $p \geq 2$; see Figure 5.

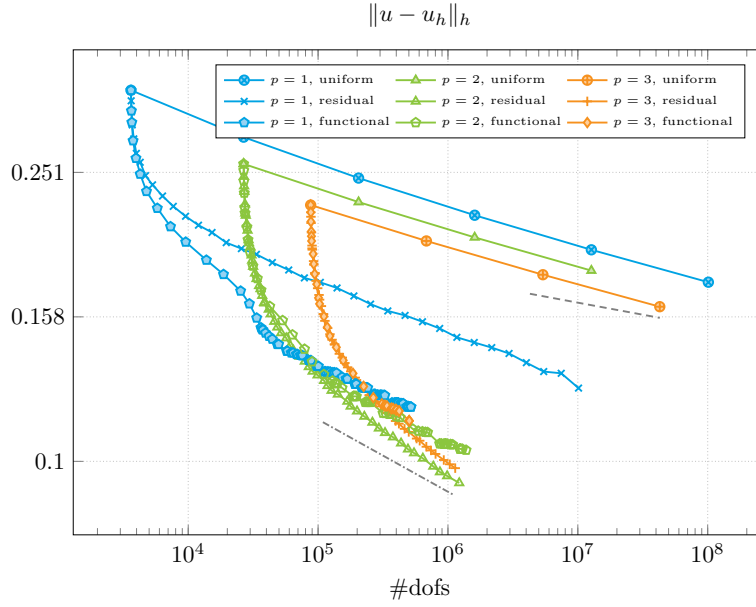


Figure 5: Example 6.3: Convergence rates for uniform and adaptive refinement, with bulk parameter $\Xi = 0.25$. The ---- line corresponds to a rate of $\mathcal{O}(N_h^{-0.1/3})$, and the -.-.- line to $\mathcal{O}(N_h^{-0.3/3})$.

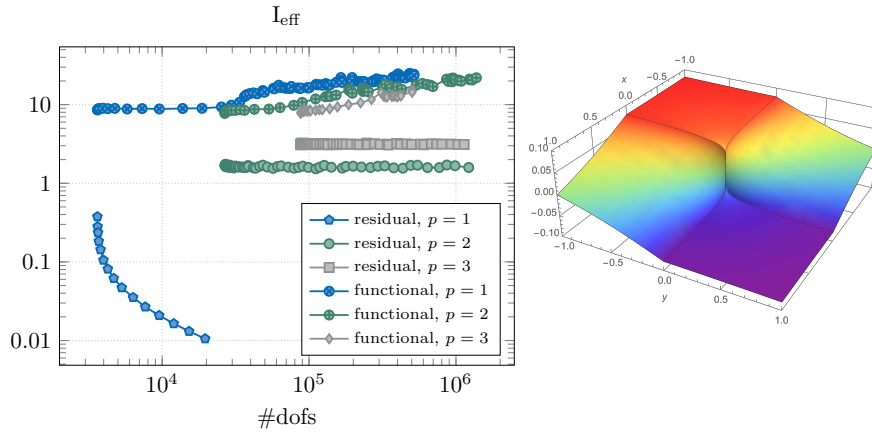


Figure 6: Example 6.3: Efficiency indices (left); and plot of the solution at $t = 1$ (right); with marking threshold $\Xi = 0.25$.

7 Conclusions

We presented and analyzed locally stabilized, consistent, conforming finite element schemes on completely unstructured simplicial space-time meshes for non-autonomous parabolic initial-boundary value problems. We admitted special distributional right-hand sides and (diffusion) coefficients which can be discontinuous in space and time. Such data can lead to low-regularity solutions. We derived a priori estimates for solutions belonging to $H^k(Q)$ with some $k \in (1, 2]$. In this case, uniform mesh refinement leads to low convergence rates. More precisely, in the energy norm $\|\cdot\|_h$, we get $O(h^{k-1})$ independently of the polynomial degree p of the shape functions used on the reference element. This theoretical result is confirmed by all numerical experiments performed. The convergence rate can drastically be improved by adaptivity. In order to devise an adaptive finite element scheme, one needs a local error indicator derived from a posteriori discretization error estimators. In contrast to elliptic boundary-value problems where adaptive finite element schemes are well established in theory and practice, the picture is different with respect to fully adaptive space-time finite element methods. We numerically studied the residual indicator proposed by O. Steinbach and H. Yang, and indicators based on functional a posteriori estimators proposed by S. Repin, where we only used the first part of the majorant as local error indicator. This choice already yields an indicator that is reliable and provides an upper bound with efficiency indices that are close to 1 for the first two examples, whereas the residual indicator is only reliable for higher polynomial degrees, with efficiency indices much bigger than 1. However, for the third example, the residual indicator results in much better efficiency indices than the functional estimator/indicator. The reduced performance of the latter is most likely due to two reasons: first, we only use the continuous finite element spaces $(V_h)^d$ for flux recovering that do not reflect the right behaviour of the fluxes across material interfaces that arise in the third example, and second, the singularity is highly anisotropic in space and time, i.e., we would need a very high spatial resolution, but relatively coarse one in time. Anisotropic refinement techniques, in particular, on simplicial space-time meshes is certainly a challenge that will be a topic of our future research on space-time adaptivity.

8 Acknowledgment

The authors would like to thank the Austrian Science Fund (FWF) for the financial support under the grant DK W1214-04. Furthermore, we would like to thank Sergey Repin for discussing with us the use of functional error estimates during his visits at Linz. Andreas Schafelner wants to thank Panayot Vassilevski for the support during his visits at the Lawrence Livermore National Laboratory, for many fruitful discussions, and for the possibility to compute on the distributed memory cluster Quartz in Livermore.

References

- [1] BANK, R. E., VASSILEVSKI, P. S., AND ZIKATANOV, L. T. Arbitrary dimension convection-diffusion schemes for space-time discretizations. *J. Comput. Appl. Math.* 310 (2017), 19–31.
- [2] BEHR, M. Simplex space-time meshes in finite element simulations. *Internat. J. Numer. Methods Fluids* 57 (2008), 1421–1434.
- [3] BERGH, J., AND LÖFSTRÖM, J. *Interpolation spaces. An introduction.*, vol. 223. Springer, Berlin, 1976.
- [4] BRAESS, D. *Finite Elemente. Theorie, schnelle Löser und Anwendungen in der Elastizitätstheorie.*, 5th revised ed. Springer Spektrum, Berlin, 2013.
- [5] BRENNER, S. C., AND SCOTT, L. R. *The mathematical theory of finite element methods*, third ed., vol. 15 of *Texts in Applied Mathematics*. Springer, New York, 2008.
- [6] CARRATURO, M., GIANNELLI, C., REALI, A., AND VÀZQUEZ, R. Suitably graded THB-spline refinement and coarsening: Towards an adaptive isogeometric analysis of additive manufacturing processes. *Comput. Methods Appl. Mech. Engrg.* 348 (2019), 660–679.
- [7] CARSTENSEN, C., FEISCHL, M., PAGE, M., AND PRAETORIUS, C. Axioms of adaptivity. *Comput. Methods Appl. Math.* 67 (2014), 1195–1253.
- [8] CIARLET, P. G. *The finite element method for elliptic problems*. North-Holland Publishing Co., Amsterdam-New York-Oxford, 1978.
- [9] C. JOHNSON, AND SARANEN, J. Streamline diffusion methods for the incompressible Euler and Navier-Stokes equations. *Math. Comp.* 47, 175 (1986), 1–18.
- [10] CLÉMENT, P. Approximation by finite element functions using local regularization. *Rev. Française Automat. Informat. Recherche Opérationnelle Sér. 9*, R-2 (1975), 77–84.
- [11] DEVAUD, D., AND SCHWAB, C. Space-time hp-approximation of parabolic equations. *Calcolo* 55, 3 (2018), 35.
- [12] DIER, D. Non-autonomous maximal regularity for forms of bounded variation. *J. Math. Anal. Appl.* 425 (2015), 33–54.
- [13] DÖRFLER, W. A convergent adaptive algorithm for Poisson’s equation. *SIAM J. Numer. Anal.* 33, 3 (1996), 1106–1124.
- [14] GANDER, M. J. 50 years of time parallel integration. In *Multiple Shooting and Time Domain Decomposition*. Springer Verlag, Heidelberg, Berlin, 2015, pp. 69–114.

- [15] HEUER, N. On the equivalence of fractional-order Sobolev semi-norms. *J. Math. Anal. Appl.* 417, 2 (2014), 505–518.
- [16] HUGHES, T., AND BROOKS, A. A multidimensional upwind scheme with no crosswind diffusion. In *Finite Element Methods for Convection Dominated Flows* (New York, 1979), T. Hughes, Ed., vol. 34 of AMD, ASME.
- [17] HUGHES, T., FRANCA, L., AND HULBERT, G. A new finite element formulation for computational fluid dynamics: VIII. The Galerkin/least-squares method for advection-diffusive equations. *Comput. Methods Appl. Mech. Engrg.* 73 (1989), 173–189.
- [18] KARYOFYLLI, V., WENDLING, L., MAKE, M., HOSTERS, N., AND BEHR, M. Simplex space-time meshes in thermally coupled two-phase flow simulations of mold filling. *Computers and Fluids* (2019), 104261.
- [19] KELLOGG, R. B. On the Poisson equation with intersecting interfaces. *Appl. Anal.* 4 (1974), 101–129.
- [20] LADYŽHENSKAYA, O. On solvability of the basic boundary value problems of parabolic and hyperbolic type. *Dokl. Akad. Nauk SSSR* 97 (1954), 395–398. (in Russian).
- [21] LADYŽHENSKAYA, O. A. *The boundary value problems of mathematical physics*, vol. 49 of *Applied Mathematical Sciences*. Springer-Verlag, New York, 1985. Translated from the Russian edition, Nauka, Moscow, 1973.
- [22] LADYZHENSKAYA, O. A., SOLONNIKOV, V. A., AND URALTSEVA, N. *Linear and quasilinear equations of parabolic type*. Nauka, Moscow, 1967.
- [23] LANGER, U., MOORE, S., AND NEUMÜLLER, M. Space-time isogeometric analysis of parabolic evolution equations. *Comput. Methods Appl. Mech. Engrg.* 306 (2016), 342–363.
- [24] LANGER, U., NEUMÜLLER, M., AND SCHAFELNER, A. Space-time Finite Element Methods for Parabolic Evolution Problems with Variable Coefficients. In *Advanced Finite Element Methods with Applications - Selected Papers from the 30th Chemnitz Finite Element Symposium 2017*, T. Apel, U. Langer, A. Meyer, and O. Steinbach, Eds., vol. 128 of *Lecture Notes in Computational Science and Engineering (LNCSE)*. Springer, Berlin, Heidelberg, New York, 2019, ch. 13, pp. 247–275.
- [25] LIONS, J. L. *Optimal control of systems governed by partial differential equations.*, vol. 170. Springer, Berlin, 1971.
- [26] MANTZAFLARIS, A., SCHOLZ, F., AND TOULOPOULOS, I. Low-rank space-time decoupled isogeometric analysis for parabolic problems with varying coefficients. *Comput. Methods Appl. Math.* 19, 1 (2019), 123–136.
- [27] MFEM: Modular finite element methods library. mfem.org.

- [28] PFEILER, C.-M., AND PRAETORIUS, D. Dörfler marking with minimal cardinality is a linear complexity problem, 2019. arXiv:1907.13078.
- [29] PYRHÖNEN, J., JOKINEN, T., AND HRABOVCOVÁ, V. *Design of Rotating Electrical Machines*. John Wiley & Sons, 2008.
- [30] REPIN, S. Estimates of deviations from exact solutions of initial-boundary value problem for the heat equation. *Rend. Mat. Acc. Lincei* 13, 9 (2002), 121–133.
- [31] REPIN, S. *A posteriori estimates for partial differential equations*, vol. 4 of *Radon Series on Computational and Applied Mathematics*. de Gruyter, Berlin, 2008.
- [32] SAAD, Y. A flexible inner-outer preconditioned GMRES algorithm. *SIAM J. Sci. Comput.* 14, 2 (1993), 461–469.
- [33] SCOTT, L. R., AND ZHANG, S. Finite element interpolation of nonsmooth functions satisfying boundary conditions. *Math. Comput.* 54, 190 (1990), 483–493.
- [34] STEINBACH, O. Space-time finite element methods for parabolic problems. *Comput. Methods Appl. Math.* 15, 4 (2015), 551–566.
- [35] STEINBACH, O., AND YANG, H. Comparison of algebraic multigrid methods for an adaptive space-time finite-element discretization of the heat equation in 3d and 4d. *Numer. Linear Algebra Appl.* 25, 3 (2018), e2143 nla.2143.
- [36] STEINBACH, O., AND YANG, H. Space-time finite element methods for parabolic evolution equations: Discretization, a posteriori error estimation, adaptivity and solution. In *Space-Time Methods: Application to Partial Differential Equations*, vol. 25 of *Radon Series on Computational and Applied Mathematics*. de Gruyter, 2019, pp. 207–248.
- [37] ZIENKIEWICZ, O. C., AND ZHU, J. Z. The superconvergent patch recovery and a posteriori error estimates. I: The recovery technique. *Int. J. Numer. Methods Eng.* 33, 7 (1992), 1331–1364.
- [38] ZIENKIEWICZ, O. C., AND ZHU, J. Z. The superconvergent patch recovery and a posteriori error estimates. II: Error estimates and adaptivity. *Int. J. Numer. Methods Eng.* 33, 7 (1992), 1365–1382.